

Pressure-enhanced splitting of density wave transitions in $\text{La}_3\text{Ni}_2\text{O}_{7-\delta}$

Received: 15 February 2024

Accepted: 5 December 2024

Published online: 17 February 2025

 Check for updates

Rustem Khasanov¹✉, Thomas J. Hicken¹, Dariusz J. Gawryluk¹,
Vahid Sazgari¹, Igor Plokhikh¹, Loïc Pierre Sorel¹, Marek Bartkowiak¹,
Steffen Bötzel², Frank Lechermann², Ilya M. Eremin², Hubertus Luetkens¹ &
Zurab Guguchia¹

The observation of superconductivity in $\text{La}_3\text{Ni}_2\text{O}_{7-\delta}$ under pressure, following the suppression of a high-temperature density wave state, has attracted considerable attention. The nature of this density wave order was not clearly identified. Here we probe the magnetic response of the zero-pressure phase of $\text{La}_3\text{Ni}_2\text{O}_{7-\delta}$ as hydrostatic pressure is applied, and find that the apparent single density wave transition at zero applied pressure splits into two. The comparison of our muon-spin rotation and relaxation experiments with dipole-field numerical analysis reveals the magnetic structure's compatibility with a stripe-type arrangement of Ni moments, characterized by alternating lines of magnetic moments and non-magnetic stripes at ambient pressure. When pressure is applied, the magnetic ordering temperature increases, whereas the unidentified density wave transition temperature falls. Our findings reveal that the ground state of the $\text{La}_3\text{Ni}_2\text{O}_{7-\delta}$ system is characterized by the coexistence of two distinct orders—a magnetically ordered spin density wave and a lower-temperature ordering that is most probably a charge density wave—with a notable pressure-enhanced separation between them.

The discovery of superconductivity in $\text{La}_3\text{Ni}_2\text{O}_{7-\delta}$ under pressure (p) has attracted notable attention^{1–5}. This interest is accentuated by the material's critical temperature $T_c \simeq 80$ K, which is above the boiling point of liquid nitrogen, positioning $\text{La}_3\text{Ni}_2\text{O}_{7-\delta}$ within the category of high-temperature superconducting materials. A recent study⁴ suggests that superconductivity in $\text{La}_3\text{Ni}_2\text{O}_{7-\delta}$ emerges on the suppression of a competing density wave (DW) order. In particular, it was found that the DW-like anomaly in resistivity, which sets in at ambient pressure at around $T_{\text{DW}} \simeq 140$ K, is progressively suppressed with increasing p , whereas the onset of a superconducting transition emerges at $p \simeq 7$ GPa (Fig. 1). Similar DW anomalies were detected at ambient pressure in specific heat and magnetization experiments^{6,7}, as well as by means of nuclear magnetic resonance^{8,9}. However, the origin of the competing DW order remains a matter of ongoing investigations. Charge ordering in NiO_2 planes induced by oxygen orderings^{10,11}, or charge

DW instabilities induced by one-dimensional Fermi surface nesting^{6,12}, were suggested to account for these anomalies. However, there is no direct evidence for the charge ordering in $\text{La}_3\text{Ni}_2\text{O}_{7-\delta}$ reported up to now. A more recent work¹³ reported the observation of a spin DW (SDW) type of order in $\text{La}_3\text{Ni}_2\text{O}_{7-\delta}$ by means of the muon-spin rotation/relaxation (μSR) technique. The ambient-pressure zero-field μSR experiments reveal the presence of static long-range magnetic order with the transition temperature of $T_N \simeq 148$ K. The SDW ordering was further confirmed by the resonant inelastic X-rays scattering¹⁴ and nuclear magnetic resonance experiments¹⁵.

Consequently, a question arises: whether the competing DW order is magnetic in origin, as suggested by the similar ambient-pressure values of DW transition temperatures $T_{\text{DW}} \simeq 140$ – 150 K (refs. 4,6–9,16,17) and $T_{\text{SDW}} \simeq 150$ K (refs. 13,15), or is the unspecified DW different in origin and coexisting with the SDW? In particular,

¹PSI Center for Neutron and Muon Sciences CNM, Paul Scherrer Institut, Villigen PSI, Switzerland. ²Theoretische Physik III, Ruhr-Universität Bochum, Bochum, Germany. ✉e-mail: rustem.khasanov@psi.ch

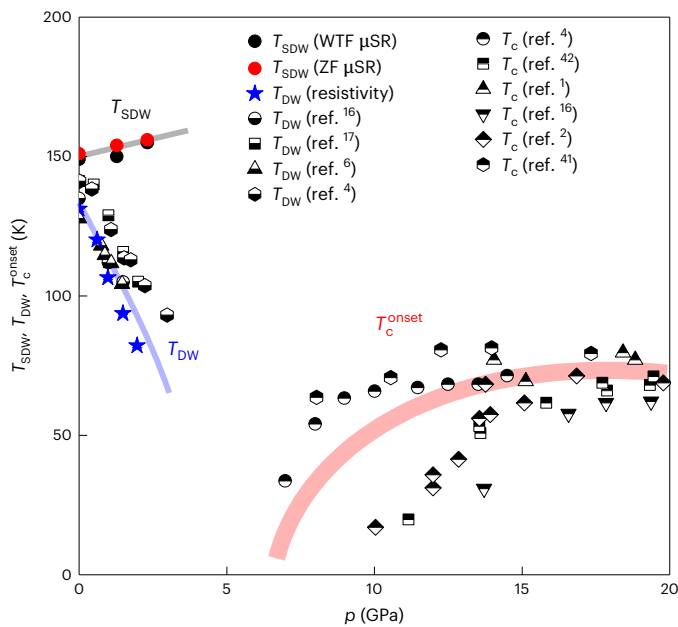


Fig. 1 | Conjectured pressure–temperature (p – T) phase diagram of $\text{La}_3\text{Ni}_2\text{O}_{7-\delta}$. The solid symbols represent pressure dependence of the SDW ordering temperature (T_{SDW}) as obtained in ZF and WTF μSR experiments (closed red and black circles) and the DW ordering temperature (T_{DW}) obtained in resistivity studies (blue stars) in the present work. The half-down filled symbols are T_{DW} versus p data^{4,6,16,17}. The half-up filled symbols represent the pressure dependence of the onset of the superconducting transition temperature $T_{\text{c}}^{\text{onset}}$ (refs. 1–4, 16, 41, 42). The lines are guides for the eye.

in the single-layer La_2NiO_4 and three-layer $\text{La}_4\text{Ni}_3\text{O}_{10}$ Ruddlesden–Popper lanthanum nickelates, the coexistent spin and charge orders were detected^{18,19}. In order to address this question, in this work, comprehensive μSR and resistivity experiments under hydrostatic pressure conditions were performed. The primary aim was to determine whether or not the SDW order follows the same pressure dependence as the DW order. At ambient pressure, our results corroborate the findings of other work^{13,15}, in which an SDW type of magnetism was detected with a transition temperature of $T_{\text{N}} \approx 151$ K. The DW transition, corresponding to the local minimum on the resistivity curve, sets 20 K lower at $T_{\text{DW}} \approx 131$ K. Under increasing pressure, the magnetic ordering temperature was observed to rise at a rate of $dT_{\text{N}}/dp \approx 2.8$ K GPa^{-1} , which is not only opposite in sign but also substantially smaller in magnitude compared with $dT_{\text{DW}}/dp \approx -26$ K GPa^{-1} (Fig. 1). The comparison of our experimental data with magnetic-dipole-field calculations also corroborates the notion of coexisting magnetic SDW and non-magnetic DW orders. Both these observations suggest that the competing DW order, which is suggested to compete with superconductivity in $\text{La}_3\text{Ni}_2\text{O}_{7-\delta}$, is probably non-magnetic in origin. These results contribute to a deeper understanding of the intricate relationship between magnetism and superconductivity in this complex oxide, offering new insights into the nature of the competing phases in high-temperature superconductors.

Results

Ambient-pressure μSR

The zero-applied-field (ZF) μSR response of $\text{La}_3\text{Ni}_2\text{O}_{7-\delta}$ measured at ambient pressure at $T = 10$ K is presented in Fig. 2. Figure 2a,b shows the ZF asymmetry spectra, representing the time evolution of the muon-spin polarization and the Fourier transformation showing the distribution of the internal fields, respectively.

The data were analysed by using equations (2) and (3) described in the Methods. The fit results reveal that the transversal part of

equation (3) consists of three terms: the fast-precessing, slow-precessing and non-precessing fast-relaxing ones (Fig. 2b show the notations). The corresponding internal fields (labelled B_{int}) at $T = 10$ K are 0.15 T, 0.01 T and 0 T. This is reminiscent of the low- T ($T \lesssim 40$ K) ZF μSR results of LaFeAsO (that is, the parent compound of the 1111 family of Fe-based superconductors) consisting of three magnetic components with the corresponding internal-field values of 0.17 T, 0.02 T and 0 T (ref. 20). Note that the fit with the simple cosine type of oscillating functions (equation (3)) suggests the consistency of our ZF μSR data with the commensurate magnetic order (Supplementary Note 4 and Supplementary Fig. 3).

The temperature evolution of the magnetic fractions is presented in Fig. 2c. The analysis reveals that for $T \lesssim 150$ K, approximately 90% of the full asymmetry is assigned to the magnetic contribution. Considering that the remaining 10% might be partially explained by the contribution of muons stopped outside the sample (3–5%, in line with the sample dimensions and GPS (general purpose surface) muon spectrometer characteristics²¹) as well as by muons stopped within the lanthanum silica apatite impurity phase (of the order of 8%; Supplementary Note 1 and Supplementary Fig. 1), this suggests that magnetism in the $\text{La}_3\text{Ni}_2\text{O}_{7-\delta}$ sample studied here is representative for the bulk. The transition from the magnetic to the non-magnetic state (from $f_{\text{m}} \approx 0.9$ to $f_{\text{m}} = 0$) is rather sharp, thereby suggesting that magnetism in $\text{La}_3\text{Ni}_2\text{O}_{7-\delta}$ sets in homogeneously.

Figure 2c shows that the volume fraction of the slow-oscillating component remains nearly temperature independent, whereas fractions of the fast-relaxing and fast-oscillating components show opposite trends. With increasing temperature, the fast-relaxing signal develops at the expense of the fast-oscillating component (Fig. 2c).

A possible explanation is that the fast-relaxing component originates from muons that stop in highly magnetically disordered regions, thereby experiencing a large distribution of fields and dephasing quickly. Conversely, the fast-precessing component is from muons that sit in the same crystallographic site, but in regions of well-ordered magnetism. The change in amplitude suggests that as the temperature increases, the volume fraction of the disordered-type sites goes up (and hence the relaxing fraction increases) at the expense of the well-ordered regions (and hence the oscillating fraction drops). This could happen if, for example, the correlation length decreases with increasing temperature, meaning the ordered regions shrink and the disordered ones grow.

The internal magnetic field (that is, the magnetic order parameter) decreases with increasing temperature and vanishes at T_{N} (Fig. 2d). The temperature behaviours of both fast-precessing ($B_{\text{int, Fast}}$) and slow-precessing ($B_{\text{int, Slow}}$) internal fields remain nearly the same (Fig. 2d), suggesting the presence of at least two non-equivalent muon stopping sites within the magnetic unit cell of $\text{La}_3\text{Ni}_2\text{O}_{7-\delta}$. The solid line in Fig. 2b represents a fit of a phenomenological power-law function expressed as²²

$$B_{\text{int}}(T) = B_{\text{int}}(0)[1 - (T/T_{\text{N}})^{\alpha}]^{\beta} \quad (1)$$

to $B_{\text{int}}(T)$ of the fast-oscillating component. The fit results in a magnetic transition temperature of $T_{\text{N}} = 151.5(1.2)$ K and exponents $\alpha = 1.58(9)$ and $\beta = 0.26(2)$. The obtained magnetic ordering temperature is in agreement with that of recent resistivity^{4,7}, nuclear magnetic resonance^{8,15} and μSR experiments¹³. The exponent $\beta \approx 0.26$ suggests a second-order-type phase transition and is rather close to a critical exponent of 1/3 expected for three-dimensional magnetic systems²³.

Candidate magnetic structure(s) of $\text{La}_3\text{Ni}_2\text{O}_{7-\delta}$

Different magnetic ground states were proposed for $\text{La}_3\text{Ni}_2\text{O}_7$ (refs. 14, 15, 24); however, no technique has thus far provided an unambiguous determination. To explore the feasibility of candidate magnetic structures, the dipole fields at muon stopping sites were calculated.

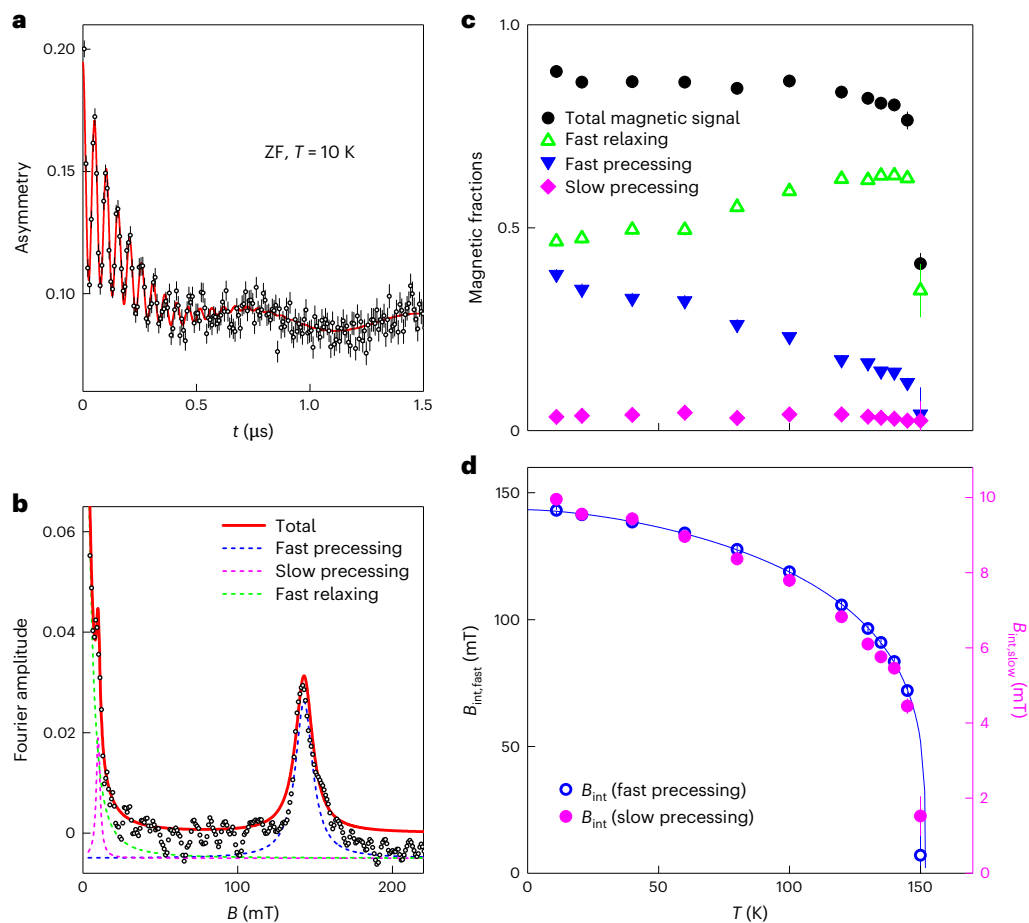


Fig. 2 | Results of ambient-pressure μ SR experiments. a, Zero-field μ SR time spectra of the $\text{La}_3\text{Ni}_2\text{O}_{7-\delta}$ sample measured at $T = 10$ K. The red line is a fit of equation (2) to the data. **b**, Fourier transform of the data presented in **a**. The dashed lines represent individual fit components. **c**, T dependencies of the ZF μ SR signal fractions. **d**, T dependencies of the internal field of the fast-precessing

and slow-precessing components. The solid line is the fit of the power law (equation (1)) to the $B_{\text{int,fast}}(T)$ data. The displayed error bars for parameters obtained from the μ SR data correspond to one standard deviation from the χ^2 fits.

The proposed structures focus on Ni moment arrangement within the a - b plane, which leaves a large number of possible configurations both due to possible different c -axis stacking patterns (where weak intra-layer coupling was suggested¹⁴) and by changing the moment direction. Varying either of these parameters does not qualitatively change the results; therefore, the best match to experiment for different a - b plane configurations is presented in Fig. 3. One important result is that some of the Ni sites lack a magnetic moment; otherwise, the slow-precessing component (corresponding to a low magnetic field at the muon site) is not observed. This suggests that $\text{La}_3\text{Ni}_2\text{O}_7$ must host charge DW and SDW, analogous to a stripe-type order in cuprate high-temperature superconductors.

There are two proposed arrangements of the missing moments, the first (Fig. 3c) with two adjacent lines of vacancies in the [110] direction, and the second (Fig. 3d) with only one line separated by the lines of moments. Experimentally, $B_{\text{int,fast}}/B_{\text{int,slow}} \approx 15$ (Fig. 2c), which can be obtained for either vacancy structure by varying the c -axis stacking and moment direction. The moment carried by Ni (m_{Ni}) might be estimated from the magnitude of the field at the muon site (Supplementary Note 8 and Supplementary Table II). If the moment points in the a - b plane, then $m_{\text{Ni}} = 0.48 - 0.67\mu_{\text{B}}$, in good agreement with the fluctuating moment of $m_{\text{Ni}} = 0.55\mu_{\text{B}}$ (ref. 25). Conversely, a lower value is required if the moment points parallel to the c axis, namely, $m_{\text{Ni}} = 0.28 - 0.31\mu_{\text{B}}$. In addition, our calculations exclude all the magnetic structure models without zero-moment lines, that is, models with magnetic moments on

all the Ni sites, as these consistently would not exhibit low-field muon sites in contrast to our experimental observation (Fig. 3c,e).

A long-range commensurate magnetic order with the ordered moments ranging from $0.3\mu_{\text{B}}$ to $0.7\mu_{\text{B}}$ should be detected by neutron experiments. The fact that neutrons do not see the magnetic order²⁴ might be related to the difference in correlation length between μ SR and neutron techniques. Muons are known to require a shorter coherence length in order to obtain an oscillatory signal^{26,27}. An indirect confirmation of a short magnetic coherence length in $\text{La}_3\text{Ni}_2\text{O}_7$ might be the presence of the non-oscillating fast-relaxing component, which increases as it approaches T_{N} (Fig. 2b,c). It seems that the short magnetic correlation length limits the amount of coherent magnetic fraction already at low temperatures, whereas the development of the fast-relaxing signal at the expense of the fast-oscillating component suggests further shortening of the coherence length as a function of temperature.

To proceed further with possible magnetic structures, the spin susceptibility at ambient pressure in the paramagnetic state was calculated within the framework of a tight-binding parameterization²⁸. Note that in bilayer systems, like $\text{La}_3\text{Ni}_2\text{O}_7$, the spin susceptibility can be decomposed into the even ($\chi_{\text{S}}^{\text{even}}$) and odd ($\chi_{\text{S}}^{\text{odd}}$) channels following the scheme outlined elsewhere²⁹. The resulting $\chi_{\text{S}}^{\text{odd}}$ and $\chi_{\text{S}}^{\text{even}}$ components of the spin susceptibility are presented in Fig. 3f. The details of the calculations are provided in Supplementary Note 9. The dominant peak in odd susceptibility is connected to scattering between the

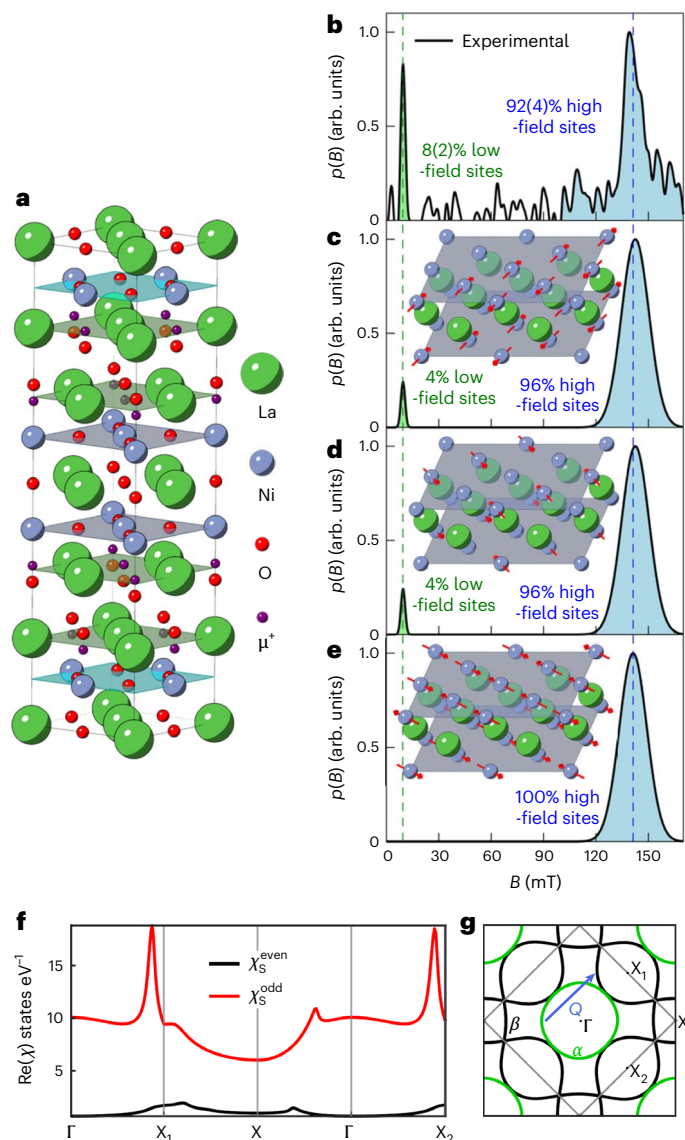


Fig. 3 | Candidate magnetic structures of $\text{La}_3\text{Ni}_2\text{O}_{7-\delta}$. **a**, Muon stopping sites as calculated with DFT + μ . Despite all the shown sites being crystallographically equivalent, for some magnetic structures, they are not magnetically equivalent. The Ni and La planes are highlighted in different colours. **b**, Magnetic-field distribution $p(B)$ (from Fig. 2b), but with the zero-field peak removed, highlights two internal fields seen by muons. **c–e**, Simulations of $p(B)$ values for different magnetic configurations. The magnetic unit cells are shown as the insets. O atoms are hidden for clarity. **f**, Spin susceptibility for the tight-binding parameterization²⁸. **g**, Fermi surface and dominant scattering vector $\mathbf{Q}_{\text{SDW}} \approx X_1$.

bonding (α) and antibonding (β) bands, and it peaks near the wave-vector $\mathbf{Q}_{\text{SDW}} \approx (\pi/2, \pi/2) = X_1$, which is visualized within the pseudotetragonal description¹⁴ in Fig. 3g. Peaks around $X_1 = (\pi/2, \pi/2)$ and $X_2 = (\pi/2, -\pi/2)$ are slightly different in magnitudes due to the intrinsic orthorhombicity in the system, making instability along X_1 more preferable. The peak at \mathbf{Q}_{SDW} implies instability towards the double stripe order within each layer and, as it occurs in the odd-spin channel (that is, for $q_z = \pi/d$, where d is the thickness of the bilayer sandwich), the antiferromagnetic coupling between the stripes along the c direction. Note that to project magnetization into real space and make comparisons with our experimental finding, the magnetization on the lattice can be written as $\vec{M}_1(\mathbf{R}_j) = \vec{\Delta}_{\text{SDW}} \cos(\mathbf{Q}_{\text{SDW}} \mathbf{R}_j + \pi/4)$ (Fig. 3e) and $\vec{M}_2(\mathbf{R}_j) = \vec{\Delta}_{\text{SDW}} \cos(\mathbf{Q}_{\text{SDW}} \mathbf{R}_j + \pi/2)$ (Fig. 3d), but requires the inclusion of higher harmonics (Fig. 3c) as $\vec{M}_3(\mathbf{R}_j) = \vec{\Delta}_{\text{SDW}} [\sqrt{2} \cos(\mathbf{Q}_{\text{SDW}} \mathbf{R}_j + \pi/4) + \cos(2\mathbf{Q}_{\text{SDW}} \mathbf{R}_j)]$.

High-pressure μ SR and resistivity experiments

The μ SR experiments under quasi-hydrostatic pressure conditions were performed at pressures of $p = 0$ GPa, 1.28 GPa and 2.31 GPa. Two sets of experiments were conducted: the first with a weak (5 mT) magnetic field applied perpendicular to the initial muon-spin polarization (weak transverse field (WTF)) and the second performed under ZF. The details of the ZF μ SR and WTF μ SR data analysis procedures, as well as the determination of the magnetic ordering temperature from WTF μ SR data ($T_{\text{N,WTF}}$), are discussed in Supplementary Notes 4 and 5.

Temperature dependencies of the internal field of the fast-precessing component ($B_{\text{int,Fast}}$) measured at various pressures are presented in Fig. 4. The solid lines correspond to the fit of equation (1) to the $B_{\text{int}}(T)$ data. To avoid the high sensitivity of the fit parameters (that is, $B_{\text{int}}(0)$ and T_{N}) to the values of exponents α and β , they were fixed at $\alpha = 1.58$ and $\beta = 0.26$ as obtained in the ambient-pressure studies (as discussed earlier and shown in Figs. 2d and 4a). The pressure dependencies of the fit parameters, namely, the magnetic ordering temperatures $T_{\text{N,WTF}}$, $T_{\text{N,ZF}}$ and the zero-temperature value of the internal field $B_{\text{int}}(0)$, are plotted in Fig. 4b,c. Both T_{N} values, as determined in the WTF μ SR and ZF μ SR experiments, increase with increasing pressure. The linear fits result in equal slopes with $dT_{\text{N}}/dp = 2.8(3)$ K GPa⁻¹. The internal field, which is proportional to the value of the ordered magnetic moment on the Ni site ($B_{\text{int}}(0) \propto m_{\text{Ni}}$), shows different tendencies. The ordered moment is nearly pressure independent, or may even slightly decrease with increasing pressure as $d \ln[B_{\text{int}}(0)]/dp \approx d \ln[m_{\text{Ni}}]/dp \approx -0.3\%$ GPa⁻¹ (Fig. 4c).

The resistivity (ρ) under pressure experiments were performed at pressures of $p = 0$ GPa, 0.61 GPa, 0.98 GPa, 1.49 GPa and 1.97 GPa (Fig. 5). Following refs. 4,6,6–9,16,17, the local minima in $\rho(T)$ could be associated with the DW transition of unknown origin. The DW transition temperature T_{DW} was obtained from parabolic fits of $\rho(T)$ in the vicinity of the local minima and it is plotted in Fig. 5b. T_{DW} decreases with increasing pressure as $T_{\text{DW}}(p) = 132.3(1.6) - p \times 25.7(1.2)$.

Our pressure data suggest that the DW order of unknown origin detected in resistivity experiments differs from the SDW magnetic order probed by means of μ SR. Indeed, (1) the ambient-pressure value of the DW transition temperature ($T_{\text{DW}}(p=0) \approx 131$ K) is approximately 20 K lower compared with the SDW one ($T_{\text{SDW}}(p=0) \approx 151$ K), and (2) the SDW and DW ordering temperatures have opposite pressure behaviours. T_{SDW} increases with increasing pressure by approaching $T_{\text{N}} \approx 155$ K at 2.31 GPa, whereas T_{DW} decreases to $T_{\text{DW}} \approx 82$ K at $p = 1.97$ GPa. Pressure, therefore, enhances the split between SDW and DW transitions from 20 K at $p = 0$ to 70 K at $p \approx 2.0$ GPa.

Discussion

The discovery of superconductivity in $\text{Nd}_{0.8}\text{Sr}_{0.2}\text{NiO}_2$ films³⁰ and in bulk $\text{La}_3\text{Ni}_2\text{O}_{7-\delta}$ under pressure¹ has sparked notable research interest in unravelling the pairing mechanism in nickel oxide systems. This discovery raises a crucial question: are the mechanisms governing superconductivity in nickelates analogous to those observed in copper oxide superconductors?

In copper oxide superconductors, the phase diagram includes spin and charge orders alongside superconductivity, and it is widely acknowledged that static and dynamic spin and charge orders play pivotal roles in the superconductivity mechanism^{31–37}. Elucidating competing orders in various nickel oxides is crucial for a comprehensive understanding of their electronic properties. In a similar vein, prior studies have revealed the presence of two distinct types of order in non-superconducting nickelate materials like $\text{La}_{2-x}\text{Sr}_x\text{NiO}_4$ (ref. 38), $\text{La}_4\text{Ni}_3\text{O}_{10}$ (ref. 19) and hole-doped $\text{La}_4\text{Ni}_3\text{O}_8$ (refs. 39,40). Crucially, the ground state of $\text{La}_3\text{Ni}_2\text{O}_{7-\delta}$ also displays characteristics associated with a DW-like order^{4,6–9,13}. This intriguing scenario is particularly noteworthy because these conditions align with those conducive to the emergence of high-temperature superconductivity in this material. This is evidenced by the suppression of a DW-like anomaly

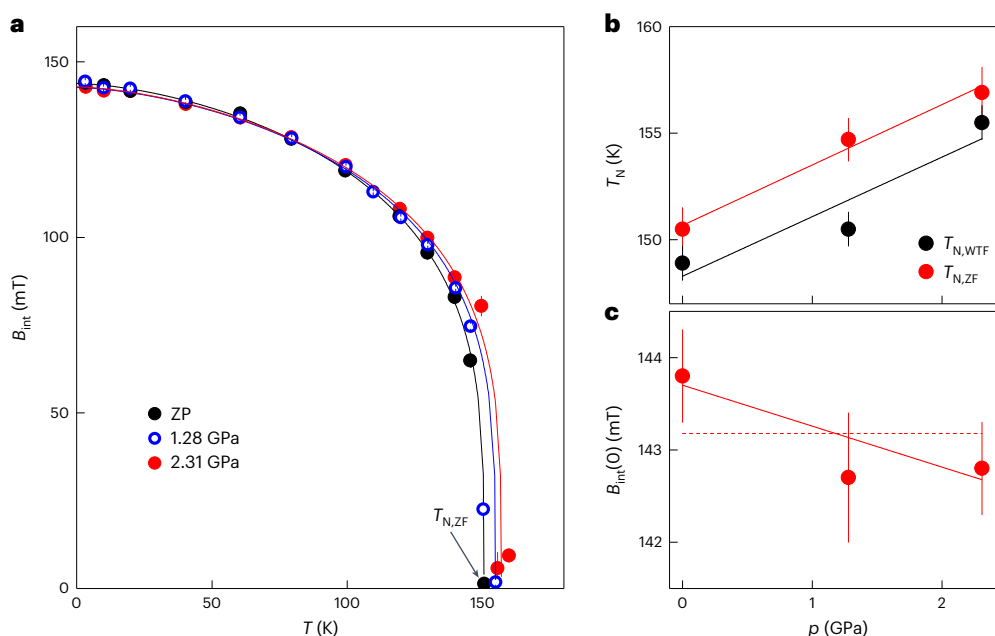


Fig. 4 | Pressure evolution of SDW order. **a**, Temperature dependencies of the internal field of the fast-precessing component measured at pressures of $p = 0$ GPa (ZP), 1.28 GPa and 2.31 GPa. **b**, Pressure dependencies of the magnetic ordering temperatures as determined in WTF μ SR and ZF μ SR experiments. The solid lines are linear fits with $T_{N,WTF}(p) = 148.3(1.5) + p \times 2.8(4)$ and

$T_{N,ZF} = 150.7(5) + p \times 2.8(3)$. **c**, Pressure dependence of the internal field of the fast-precessing component. The solid and dashed lines are linear fits with $B_{int}(0, p) = 143.7(3) - p \times 0.44(22)$ and $B_{int}(0, p) = 143.2(4)$, respectively. The error bars for individual data points correspond to one standard deviation from the χ^2 fits.

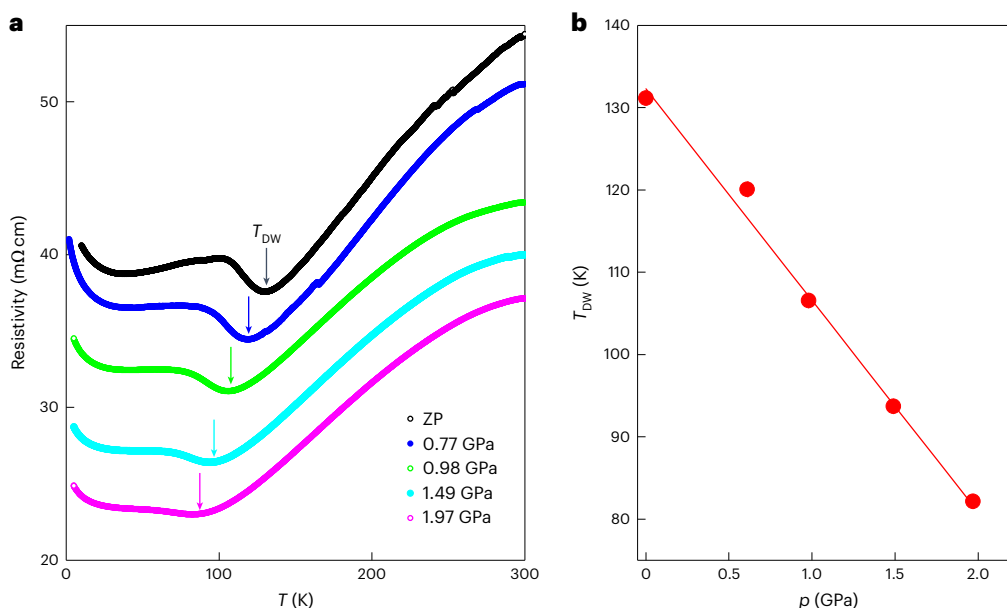


Fig. 5 | Pressure evolution of the DW order. **a**, Temperature dependencies of the resistivity measured at pressures of $p = 0$ GPa, 0.61 GPa, 0.98 GPa, 1.49 GPa and 1.97 GPa. The arrows represent the DW transition temperature T_{DW} . **b**, Dependence of T_{DW} on pressure. The solid line is a linear fit: $T_{DW}(p) = 132.3(1.6) - p \times 25.7(1.2)$.

in resistivity as the material approaches the superconducting dome under pressure⁴.

Our experiments unveil the presence of commensurate magnetic order, as well as the critical temperature associated with the DW anomaly. One of the pivotal findings in our paper is the observation that pressure induces an elevation in the magnetic ordering temperature, underscoring the resilience of magnetism under external pressure. Notably, this behaviour stands in stark contrast to the substantial suppression, specifically by nearly 50 K within the same pressure range, of the transport anomaly associated with the DW instability (Fig. 5).

The distinctive pressure-induced response in $\text{La}_3\text{Ni}_2\text{O}_{7-\delta}$, as well as the results of the dipole-field calculations, implies the simultaneous existence of two separate orders in its ground state: magnetic and most likely charge DW orders. Remarkably, our results point to a pressure-enhanced decoupling between these two distinct orders. In cuprates or hole-doped nickelates like $\text{La}_{2-x}\text{Sr}_x\text{NiO}_4$, the relationship between spin and charge orders is particularly intricate, with both orders being strongly intertwined and exhibiting similar responses to external parameters. However, this intricate interplay differs in $\text{La}_3\text{Ni}_2\text{O}_{7-\delta}$, where the behaviour of spin and charge orders deviates

from this pattern. Here the response to external parameters reveals a distinct and less correlated behaviour between spin and charge orders compared with the observed intertwining in cuprates and hole-doped nickelates. This distinction underscores the unique electronic characteristics and order interplay in $\text{La}_3\text{Ni}_2\text{O}_{7-\delta}$, adding to the complexity of the superconducting mechanism in this nickel oxide system.

Online content

Any methods, additional references, Nature Portfolio reporting summaries, source data, extended data, supplementary information, acknowledgements, peer review information; details of author contributions and competing interests; and statements of data and code availability are available at <https://doi.org/10.1038/s41567-024-02754-z>.

References

- Sun, H. et al. Signatures of superconductivity near 80 K in a nickelate under high pressure. *Nature* **621**, 493–498 (2023).
- Zhang, M. et al. Effects of pressure and doping on Ruddlesden-Popper phases $\text{La}_{n+1}\text{Ni}_n\text{O}_{3n+1}$. *J. Mater. Sci. Technol.* **185**, 147–154 (2024).
- Hou, J. et al. Emergence of high-temperature superconducting phase in pressurized $\text{La}_3\text{Ni}_2\text{O}_7$ crystals. *Chinese Phys. Lett.* **40**, 117302 (2023).
- Wang, G. et al. Pressure-induced superconductivity in polycrystalline $\text{La}_3\text{Ni}_2\text{O}_7$. *Phys. Rev. X* **14**, 011040 (2024).
- Wang, M. et al. Normal and superconducting properties of $\text{La}_3\text{Ni}_2\text{O}_7$. *Chinese Phys. Lett.* <https://doi.org/10.1088/0256-307X/41/7/077402> (2024).
- Wu, G., Neumeier, J. J. & Hundley, M. F. Magnetic susceptibility, heat capacity, and pressure dependence of the electrical resistivity of $\text{La}_3\text{Ni}_2\text{O}_7$ and $\text{La}_4\text{Ni}_3\text{O}_{10}$. *Phys. Rev. B* **63**, 245120 (2001).
- Liu, Z. et al. Evidence for charge and spin density waves in single crystals of $\text{La}_3\text{Ni}_2\text{O}_7$ and $\text{La}_3\text{Ni}_2\text{O}_6$. *Sci. China: Phys., Mech. Astron.* **66**, 217411 (2023).
- Fukamachi, T., Oda, K., Kobayashi, Y., Miyashita, T. & Sato, M. Studies on successive electronic state changes in systems with NiO_2 planes— ^{139}La -NMR/NQR. *J. Phys. Soc. Jpn* **70**, 2757–2764 (2001).
- Kakoi, M. et al. Multiband metallic ground state in multilayered nickelates $\text{La}_3\text{Ni}_2\text{O}_7$ and $\text{La}_2\text{Ni}_3\text{O}_{10}$ revealed by ^{139}La -NMR at ambient pressure. *J. Phys. Soc. Jpn* **93**, 053702 (2024).
- Taniguchi, S. et al. Transport, magnetic and thermal properties of $\text{La}_3\text{Ni}_2\text{O}_{7-\delta}$. *J. Phys. Soc. Jpn* **64**, 1644–1650 (1995).
- Kobayashi, Y. et al. Transport and magnetic properties of $\text{La}_3\text{Ni}_2\text{O}_{7-\delta}$ and $\text{La}_4\text{Ni}_3\text{O}_{10-\delta}$. *J. Phys. Soc. Jpn* **65**, 3978–3982 (1996).
- Seo, D. K., Liang, W., Whangbo, M. H., Zhang, Z. & Greenblatt, M. Electronic band structure and Madelung potential study of the nickelates La_2NiO_4 , $\text{La}_3\text{Ni}_2\text{O}_7$, and $\text{La}_4\text{Ni}_3\text{O}_{10}$. *Inorg. Chem.* **35**, 6396–6400 (1996).
- Chen, K. et al. Evidence of spin density waves in $\text{La}_3\text{Ni}_2\text{O}_{7-\delta}$. *Phys. Rev. Lett.* **132**, 256503 (2024).
- Chen, X. et al. Electronic and magnetic excitations in $\text{La}_3\text{Ni}_2\text{O}_7$. *Nat. Commun.* **15**, 9597 (2024).
- Dan, Z. et al. Spin-density-wave transition in double-layer nickelate $\text{La}_3\text{Ni}_2\text{O}_7$. Preprint at <https://arxiv.org/abs/2402.03952> (2024).
- Zhang, Y. et al. High-temperature superconductivity with zero-resistance and strange metal behavior in $\text{La}_3\text{Ni}_2\text{O}_7$. *Nat. Phys.* **20**, 1269–1273 (2024).
- Hosoya, T. et al. Pressure studies on the electrical properties in $\text{R}_{2-x}\text{Sr}_x\text{Ni}_{1-y}\text{Cu}_y\text{O}_{4+\delta}$ ($\text{R}=\text{La}, \text{Nd}$) and $\text{La}_3\text{Ni}_2\text{O}_{7+\delta}$. *J. Phys. Conf. Series* **121**, 052013 (2008).
- Tranquada, J. M., Lorenzo, J. E., Buttrey, D. J. & Sachan, V. Cooperative ordering of holes and spins in $\text{La}_2\text{NiO}_{4.125}$. *Phys. Rev. B* **52**, 3581–3595 (1995).
- Zhang, J. et al. Intertwined density waves in a metallic nickelate. *Nat. Commun.* **11**, 6003 (2020).
- Klauss, H.-H. et al. Commensurate spin density wave in LaFeAsO : a local probe study. *Phys. Rev. Lett.* **101**, 077005 (2008).
- PSI. General purpose surface-muon instrument (GPS); <https://www.psi.ch/en/smus/gps>
- Pratt, F. L. et al. A μSR study of magnetic ordering and metamagnetism in a bilayered molecular magnet. *J. Phys. Condens. Matter* **19**, 456208 (2007).
- Campostrini, M., Hasenbusch, M., Pelissetto, A., Rossi, P. & Vicari, E. Critical exponents and equation of state of the three-dimensional Heisenberg universality class. *Phys. Rev. B* **65**, 144520 (2002).
- Xie, T. et al. Neutron scattering studies on the high- T_c superconductor $\text{La}_3\text{Ni}_2\text{O}_{7-\delta}$ at ambient pressure. *Sci. Bull* **69**, 3221–3227 (2024).
- Shilenko, D. A. & Leonov, I. V. Correlated electronic structure, orbital-selective behavior, and magnetic correlations in double-layer $\text{La}_3\text{Ni}_2\text{O}_7$ under pressure. *Phys. Rev. B* **108**, 125105 (2023).
- Yaouanc, A. & de Réotier, P. D. *Muon Spin Rotation, Relaxation, and Resonance* (Oxford Science Publications, 2011).
- de Réotier, P. D., Yaouanc, A. & Maisuradze, A. New insights for the description of magnetic correlations inferred from μSR . *J. Phys.: Conf. Ser.* **551**, 012005 (2014).
- Wang, Y., Jiang, K., Wang, Z., Zhang, F.-C. & Hu, J. Electronic structure and superconductivity in bilayer $\text{La}_3\text{Ni}_2\text{O}_7$. *Phys. Rev. B* **110**, 205122 (2024).
- Bötzel, S., Lechermann, F., Gondolf, J. & Eremin, I. M. Theory of magnetic excitations in multilayer nickelate superconductor $\text{La}_3\text{Ni}_2\text{O}_7$. *Phys. Rev. B* **109**, L18052 (2024).
- Li, D. et al. Superconductivity in an infinite-layer nickelate. *Nature* **572**, 624–627 (2019).
- Tranquada, J., Sternlieb, B., Axe, J., Nakamura, Y. & Uchida, S. Evidence for stripe correlations of spins and holes in copper oxide superconductors. *Nature* **375**, 561–563 (1995).
- Ghiringhelli, G. et al. Long-range incommensurate charge fluctuations in $(\text{Y,Nd})\text{Ba}_2\text{Cu}_3\text{O}_{6+x}$. *Science* **337**, 821–825 (2012).
- Chang, J. et al. Direct observation of competition between superconductivity and charge density wave order in $\text{YBa}_2\text{Cu}_3\text{O}_y$. *Nat. Phys.* **8**, 871–876 (2012).
- Fradkin, E., Kivelson, S. A. & Tranquada, J. M. Colloquium: theory of intertwined orders in high temperature superconductors. *Rev. Mod. Phys.* **87**, 457–482 (2015).
- Keimer, B., Kivelson, S. A., Norman, M. R., Uchida, S. & Zaanen, J. From quantum matter to high-temperature superconductivity in copper oxides. *Nature* **518**, 179–186 (2015).
- Kivelson, S. A. et al. How to detect fluctuating stripes in the high-temperature superconductors. *Rev. Mod. Phys.* **75**, 1201–1241 (2003).
- Guguchia, Z. et al. Using uniaxial stress to probe the relationship between competing superconducting states in a cuprate with spin-stripe order. *Phys. Rev. Lett.* **125**, 097005 (2020).
- Ricci, A. et al. Measurement of spin dynamics in a layered nickelate using X-ray photon correlation spectroscopy: evidence for intrinsic destabilization of incommensurate stripes at low temperatures. *Phys. Rev. Lett.* **127**, 057001 (2021).
- Zhang, J. et al. Stacked charge stripes in the quasi-2D trilayer nickelate $\text{La}_4\text{Ni}_3\text{O}_8$. *Proc. Natl Acad. Sci. USA* **113**, 8945–8950 (2016).
- Zhang, J. et al. Spin stripe order in a square planar trilayer nickelate. *Phys. Rev. Lett.* **122**, 247201 (2019).
- Puphal, P. et al. Unconventional crystal structure of the high-pressure superconductor $\text{La}_3\text{Ni}_2\text{O}_7$. *Phys. Rev. Lett.* **133**, 146002 (2024).
- Zhou, Y. et al. Investigations of key issues on the reproducibility of high- T_c superconductivity emerging from compressed $\text{La}_3\text{Ni}_2\text{O}_7$. Preprint at <https://arxiv.org/abs/2311.12361> (2023).

Publisher's note Springer Nature remains neutral with regard to jurisdictional claims in published maps and institutional affiliations.

Open Access This article is licensed under a Creative Commons Attribution 4.0 International License, which permits use, sharing, adaptation, distribution and reproduction in any medium or format, as long as you give appropriate credit to the original author(s) and the source, provide a link to the Creative Commons licence, and indicate if changes were made. The images or other third party material in this

article are included in the article's Creative Commons licence, unless indicated otherwise in a credit line to the material. If material is not included in the article's Creative Commons licence and your intended use is not permitted by statutory regulation or exceeds the permitted use, you will need to obtain permission directly from the copyright holder. To view a copy of this licence, visit <http://creativecommons.org/licenses/by/4.0/>.

© The Author(s) 2025

Methods

Sample preparation

The $\text{La}_3\text{Ni}_2\text{O}_{7-\delta}$ sample was synthesized by means of the solid-state reaction described in Supplementary Note 1. The X-ray diffraction studies confirm the presence of the main fraction $\text{La}_3\text{Ni}_2\text{O}_{7-\delta}$ ($\delta \approx 0$) and a small amount (of the order of 8%) of the impurity phase of lanthanum silica apatite (Supplementary Note 1 and Supplementary Fig. 1).

μ SR experiments

ZF and WTF μ SR experiments were carried out at the Paul Scherrer Institute. Experiments under ambient pressure were performed at the π E3 beamline using the GPS spectrometer⁴³. Experiments under the quasi-hydrostatic pressure conditions were conducted at the μ E1 beamline using the GPD (general purpose decay) spectrometer^{44,45}. A pressure of up to 2.3 GPa was generated in a double-walled clamp-type cell made of non-magnetic MP35N alloy⁴⁴. As a pressure-transmitting medium, Daphne 7373 oil was used.

Muon stopping sites and dipole-field calculations

The muon stopping sites in $\text{La}_3\text{Ni}_2\text{O}_7$ were calculated by means of a DFT + μ approach⁴⁶ using the MuFinder application⁴⁷. The dipole-field calculations utilized the MUESR code⁴⁸.

ZF μ SR data analysis procedure

The fit to the experimental data was performed using the following functional form:

$$A(t) = A_s [f_m P_{s,m}(t) + (1 - f_m) P_{s,nm}] + A_{bg} P_{bg}(t). \quad (2)$$

Here A_s/A_{bg} and $P_s(t)/P_{bg}(t)$ are the initial asymmetry and time evolution of the muon-spin polarization of the sample (s)/background (bg) contribution. The sample part is further divided into magnetic (m) and non-magnetic (nm) contributions, with weights f_m and $1 - f_m$, respectively, and

$$P_{s,m}(t) = \frac{2}{3} \sum_i f_i e^{-\lambda_i t} \cos(\gamma_\mu B_{int,i} t) + \frac{1}{3} e^{-\lambda t}. \quad (3)$$

Here $\gamma_\mu = 851.616 \text{ MHz T}^{-1}$ is the muon gyromagnetic ratio, λ is the exponential relaxation rate and f_i is the volume fraction of the i th magnetic component. The indices 2/3 and 1/3 account for powder averaging, where 2/3 of the muon spins precess in internal fields perpendicular (transversal (T)) to the field directions and 1/3 remain parallel (longitudinal (L)) to $B_{int,i}$ (refs. 26,49–54).

Resistivity experiments

Experiments under ambient pressure were performed by using the resistivity option hardware and software of the Quantum Design Physical Property Measurement System. Experiments under pressure were performed with the same instrument by using Almax easyLab Pcell15/30 module⁵⁵.

Inclusion and ethics

We have read the Nature Portfolio Authorship Policy and confirm that this manuscript complies with the policy information about authorship: inclusion and ethics in global research.

Data availability

Raw data are available upon request and are available at <http://musruser.psi.ch/cgi-bin/SearchDB.cgi>. Source data are provided with this paper.

References

- Amato, A. et al. The new versatile general purpose surface-muon instrument (GPS) based on silicon photomultipliers for μ SR measurements on a continuous-wave beam. *Rev. Sci. Instrum.* **88**, 093301 (2017).

- Khasanov, R. et al. High pressure research using muons at the Paul Scherrer Institute. *High Pressure Res.* **36**, 140–166 (2016).
- Khasanov, R. Perspective on muon-spin rotation/relaxation under hydrostatic pressure. *J. Appl. Phys.* **132**, 190903 (2022).
- Blundell, S. J. & Lancaster, T. DFT + μ : density functional theory for muon site determination. *Appl. Phys. Rev.* **10**, 021316 (2023).
- Huddart, B. M. et al. MuFinder: a program to determine and analyse muon stopping sites. *Comput. Phys. Commun.* **280**, 108488 (2022).
- Bonfá, P., Onuorah, IfeanyiJohn & De Renzi, R. Introduction and a quick look at MUESR, the Magnetic structure and mUON Embedding Site Refinement suite. *JPS Conf. Proc.* **21**, 011052 (2018).
- Schenck, A. *Muon Spin Rotation Spectroscopy: Principles and Applications in Solid State Physics* (Adam Hilger, 1985).
- Schenck, A. & Gygax, F. N. in *Handbook of Magnetic Materials* (ed Buschow, K. H. J.) Vol. 9 (Elsevier, 1995).
- Smilga, V. P. & Belousov, Y. M. *The Muon Method in Science* (Nova Science Publisher, 1994).
- Karlsson, E. *Solid State Phenomena, As Seen by Muons, Protons, and Excited Nuclei* (Clarendon, 1995).
- Lee, S. L., Kilcoyne, S. H. & Cywinski, R. (eds) *Muon Science: Muons in Physics, Chemistry and Materials* (IOP Publishing, 1999).
- Blundell, S. J., De Renzi, R., Lancaster, T. & Pratt, F. L. (eds) *Muon Spectroscopy. An Introduction* (Oxford Univ. Press, 2022).
- Almax easyLab. easyLab Pcell15/30; <https://almax-easylab.com/product/easylab-pcell-15-30/>

Acknowledgements

Z.G. acknowledges support from the Swiss National Science Foundation (SNSF) through SNSF Starting Grant (no. TMSG12_211750). The work of S.B., F.L. and I.M.E. is supported by the German Research Foundation within the bilateral NSFC-DFG Project ER 463/14-1.

Author contributions

R.K. conceived and supervised the project. D.J.G., I.P. and L.P.S. synthesized the sample and conducted the X-ray characterization. R.K. performed the μ SR experiments and analysed the μ SR data. T.J.H. calculated the muon stopping sites and dipole-field distributions for various possible magnetic structures. S.B., F.L. and I.M.E. calculated the spin susceptibility. V.S. and Z.G. conducted the electrical transport experiments under pressure with contribution from M.B. R.K., T.J.H. and Z.G. wrote the manuscript with contributions from D.J.G., L.P.S., S.B., F.L., I.M.E. and H.L.

Funding

Open Access funding provided by Lib4RI – Library for the Research Institutes within the ETH Domain: Eawag, Empa, PSI & WSL.

Competing interests

The authors declare no competing interests.

Additional information

Supplementary information The online version contains supplementary material available at <https://doi.org/10.1038/s41567-024-02754-z>.

Correspondence and requests for materials should be addressed to Rustem Khasanov.

Peer review information *Nature Physics* thanks the anonymous reviewers for their contribution to the peer review of this work.

Reprints and permissions information is available at www.nature.com/reprints.